Research Article | Vol. 28, No. 18 / 31 August 2020 / Optics Express 25858
Optics EXPRESS

Unveiling structured domains of persistent luminescent microparticles using second-harmonic generation microscopy

GODOFREDO BAUTISTA,[1,2] LEEVI KALLIONIEMI,[1] AND LAETICIA PETIT[1,3]

[1] Photonics Laboratory, Physics Unit, Tampere University, Korkeakoulunkatu 3, 33720, Tampere, Finland
[2] godofredo.bautista@tuni.fi
[3] laeticia.petit@tuni.fi

Abstract: We introduce the use of second-harmonic generation microscopy to investigate individual persistent luminescent microparticles that are either embedded in glass or as prepared. Three-dimensional mapping of the second-harmonic generation from monoclinic dysprosium- and europium-doped strontium aluminates, a popular persistent luminescent material, allows us to unambiguously visualize and reveal for the first time the presence of micrometer-sized structured domains from such microparticles. The technique was found to have high potential for studying noninvasively a wide range of individual persistent luminescent entities that are embedded in a variety of glass matrices.

1. Introduction

For decades, there has been a lot of fundamental and commercial interest in the syntheses, analyses and applications of persistent luminescence (PeL) entities. Such entities can store the excitation energy, and release an optical emission that lasts for several minutes to hours after the excitation is stopped [1,2]. Here, it is generally accepted that the excitation energy could be stored in traps that could be either intrinsic or intentionally introduced [3]. Due to the intriguing properties of PeL entities, they have been significantly valued as small animal imaging probes [4,5], therapeutic agents [6], drug nanocarriers [7], stress sensors [8], building blocks of commercial glow-in-the-dark materials (e.g., toys, entertainment and emergency signages) and many more [9].

While there have been many significant developments on the synthesis of PeL entities such as microparticles and nanoparticles and their characterization in the past decades, most works have depended on the structural characterization techniques of individual PeL entities and large-scale optical measurements from samples that contain an ensemble of microparticles. Although the structural, compositional and crystalline features of an individual PeL microparticle can be acquired using scanning electron microscopy (SEM) [10], X-ray diffraction [11], and energy-dispersive X-ray spectroscopy (EDS) [12], the techniques are depth discrimination-limited and always invasive, i.e., the sample always needs to undergo pre-processing and manipulation beforehand. Most importantly, the traditional spectroscopic techniques that are used to study such PeL entities have been largely based on linear optical phenomena (e.g., PeL excitation and emission spectra [2], thermoluminescence [3], Raman [13], infrared absorption [14] and X-ray absorption [15]). Even if such linear optical effects are useful, these techniques are accompanied by long acquisition times (e.g., image frame rate could reach the order of few hours), insensitivity to inherent molecular symmetries of many structures, limited spatial resolutions (e.g., image resolution could reach the order of few centimeters) and lack of optical sectioning capability. Altogether, the above drawbacks could possibly obscure the detection of pristine (or undisturbed) three-dimensional spatial information and packing of relevant molecular symmetries inside a

#398215 https://doi.org/10.1364/OE.398215
Journal © 2020 Received 22 May 2020; revised 22 Jul 2020; accepted 10 Aug 2020; published 18 Aug 2020

Optics EXPRESS

PeL microparticle. Thus, there is still a need to develop new kinds of optical techniques that can be used to probe an individual PeL microparticle in three dimensions, at high spatial resolution and, most importantly, in a noninvasive manner.

Second-harmonic generation (SHG) could be an excellent candidate to probe nondestructively the microscopic structure of PeL crystals. This is because SHG is extremely sensitive to various levels of symmetry-breaking from molecular symmetries to three-dimensional organization [16]. In SHG, two photons at the fundamental frequency are simultaneously scattered at the sample in order to create a single photon at the doubled frequency. This process is parametric so SHG microscopy technique is naturally noninvasive. Due to these remarkable features, SHG microscopy has been used to probe a wide variety of samples [17,18]. In particular, SHG microscopy has been used to study SHG-active entities that are embedded in highly symmetric environments (e.g., glass matrices and polymer films) [19–22]. SHG microscopy has been also shown to be capable of determining the point group symmetry of a variety noncentrosymmetric structures [23], discriminating polymorphic crystal forms [24], and visualizing polar domains [25–27]. To date, the investigation of an individual PeL microparticle using a nonlinear optical technique such as SHG remains lacking.

In this work, we demonstrate the use of background-free SHG microscopy to investigate individual PeL microparticles that are embedded in glass or as prepared on top of glass. Using three-dimensional mapping of the SHG signals from monoclinic dysprosium- and europium-doped strontium aluminate crystals, the presence of micrometer-sized domains from such single microparticles are unambiguously visualized and unveiled for the first time. The technique is shown to have high potential in studying noninvasively a wide range of individual persistent luminescent entities that are embedded in a variety of glass matrices.

2. Methodology

2.1. SHG microscope

To study the persistent luminescent microparticles, we used a custom-built point scanning SHG microscope (Fig. 1). Previously, we have used this microscope configuration to investigate the nonlinear optical signals from a variety of nanostructures [28–32]. In brief, a pulsed laser (wavelength of 1060 nm, pulse length of 140 fs, repetition rate of 80 MHz) is utilized. After routine beam collimation, spatial filtering and expansion, the beam is directed onto a microscope objective (numerical aperture of 0.8, 50×magnification). This objective is used to deliver further the beam into the sample, which is fixed on a three-axis piezo-scanner. This dry objective also allows us to perform nondestructive probing of hygroscopic samples including microparticles on top of it at sufficient image quality. To collect the SHG signals from the sample, the same objective is used. To distinguish the SHG signal from the excitation wavelength and other generated optical signals, high quality optical filters (e.g., shortpass (cutoff at 758.2 nm) and SHG bandpass (531 nm ± 11 nm)) were used. The background-free SHG signals are then directed onto a cooled photomultiplier tube (PMT).

The SHG from the sample is collected pixel-by-pixel, i.e., as a function of its relative three-dimensional position with respect to the focused beam. This is done via a custom-designed LabVIEW program. The pixel dwell time is 50 ms. The total acquisition time of a SHG map with 100 pixels by 100 pixels resolution is around 17 minutes. The three-dimensional scanning capability is limited by the performance of the scanning stage, which only allows imaging of an extended sample within a 75 µm × 75 µm × 50 µm volume. In all experiments, an average power of 10 mW, which was measured before the microscope objective, was used. The average power of the laser beam was set by an attenuator that is composed of a half-wave plate and a polarizing beamsplitter. Designated half- and quarter-wave plates were used before the microscope objective in order to access linear and circularly polarizations, respectively. The quality of the circularly polarized beam was verified using a beam profiler or power sensor in tandem with an analyzer.

Optics EXPRESS

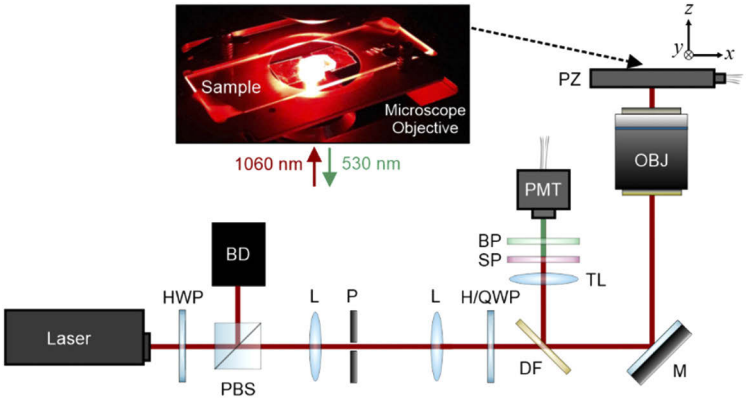

Fig. 1. Schematic diagram of the SHG microscopy setup. The SHG microscope is powered by a femtosecond laser source (1060 nm, 140 fs, 80 MHz). The other components include half-wave plate (HWP), polarizing beamsplitter (PBS), beam dump (BD), lenses (L), mirror (M), pinhole (P), quarter-wave plate (QWP), dichroic filter (DF), microscope objective (OBJ), piezo-scanners (PZ), tube lens (TL), shortpass filter (SP), bandpass filter (BP) and cooled photomultiplier tube (PMT). In the inset figure, an actual photograph of the PeL microparticle containing glass sample is illuminated from below by the femtosecond laser using the objective. The SHG signal is collected by the same objective. White light coupled to a red filter and a camera was used to find the sample before SHG scanning experiments.

Circular polarization was used mostly in all experiments (except in Figs. 3 and 4 data) in order to be have immediate sensitivity to anisotropic crystal domains in all in-plane directions. Under tight focusing geometry, the generated longitudinal electric fields at the focal volume of circular polarization are very weak and off-centered with a doughnut-like distribution. These fields are not expected to have strong effect on the SHG response of the material studied here. All measurements were performed at room temperature.

2.2. PeL sample preparation and related characterization

Our PeL system is based on a commercial photoluminescent pigment. This pigment consisted of inorganic microparticles of strontium aluminate ($SrAl_2O_4$) doped with europium and dysprosium (PYG-6L, average size of 95 ± 5 µm, Jinan Realglow Luminous Technology Co. Ltd.). $SrAl_2O_4$ was selected due to its several favorable attributes: this pigment is stable and efficient. We prepared two samples based on these PeL materials. The first sample (S1) is the as-received microparticles. For the measurement, they were glued on a standard borosilicate microscope slide using wax (Fig. 2(a)). The second sample (S2) depicted in Fig. 2(b) was obtained using the direct doping method as in Ref. [33]; the microparticles were added at 550°C in the glass

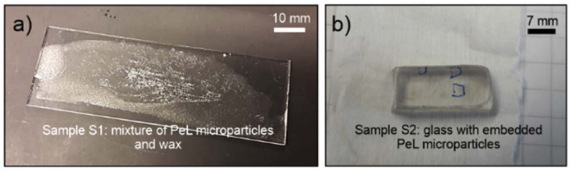

Fig. 2. Photographs of a) sample S1 with PeL microparticles glued on a standard borosilicate microscope slide and b) glass sample S2 with embedded PeL microparticles using direct doping method. The pictures were taken using phone camera under ambient light settings.

Optics EXPRESS

melt with the $90NaPO_3$-10NaF (in mol%) composition and the glass was quenched 3 min after adding the microparticles. As explained in Ref. [34], the composition of the PeL microparticles remains essentially unaltered using this method. Prior to structural characterization and SHG experiments, this glass sample was cut and polished.

In order to examine the morphology and collect the mapping of the elements in the sample S2, a scanning electron microscope (Carl Zeiss Crossbeam 540) in tandem with an EDS detector (Oxford Instruments X-MaxN 80) was used. Prior to EDS mapping, the polished glass was coated with a thin carbon layer.

3. Results and discussion

Strontium aluminate, $SrAl_2O_4$, has two crystallographic polymorphs namely; monoclinic and hexagonal. Below 650°C, strontium aluminate is stable and monoclinic belonging to space group $P2_1$ [35]. This space group is expected to have several nonvanishing second-order susceptibility tensor components [16] that is sufficient to create SHG. Indeed, it has been demonstrated that significant SHG can be detected in a relevant SHG-active monoclinic crystal systems [24,36–38].

We first performed systematic SHG experiments on sample S1, which consisted of pristine (or as prepared) PeL microparticles placed on a standard borosilicate microscope slide. Shown in Fig. 3(a) is the brightfield microscopy image of the PeL microparticle. The SHG microscopy signals (Fig. 3(b)) of a specific region of the PeL microparticle clearly stand out from the background. For this map, the set maximum of the scale bar is 10000 counts. No significant SHG was found in this particular wax material. In this measurement, the shortpass filter and the bandpass filter at 531 ± 11 nm, which is very near the expected SHG wavelength were both mounted before the PMT. To validate the nature of these nonlinear optical signals, we rescanned the same region using the same experimental parameters but with different bandpass filters. The shortpass filter is always used in order to block the fundamental wavelength. As shown below, the nonlinear optical signals detected with the other bandpass filters at (Fig. 3(c)) 500 ± 7.5 nm, (Fig. 3(d)) 560 ± 7 nm, and (Fig. 3(e)) 629 ± 28 nm were much weaker than the SHG signals. For these maps, the set maximum of the scale bar is 100 counts. It is also well-known that $SrAl_2O_4$:Eu displays a characteristic Eu^{2+} based single broad emission band peaking at 520 nm with a full width at half maximum (FWHM) of about 85 nm at room temperature. If the emission is dominated by *5d-4f* transitions in divalent europium, the scanning maps at the other bandpass filters should exhibit significant signals and microscopic features that mimic the SHG map. However, it is still likely that some of the background signals could be due to multiphoton-induced luminescence since we are using a femtosecond laser source at 1060 nm. Nevertheless, the SHG signals are still about 4 orders of magnitude higher than the signals taken with other bandpass filters. Altogether, the results show that SHG is dominant and background free, strongly validating that the main sources of SHG are originating from the PeL microparticle.

More interestingly, the SHG image in Fig. 3(b) revealed that the PeL microparticle contains structured domains of varied orientations. There is no consensus in the community about the term "structured domains" as they have been used in varied contexts (e.g., crystals, ferroelectrics, and life sciences). Here, we use structured domains to refer to regions in crystal that exhibit similar characteristics such as orientation. This is strongly linked to how the molecules in that region are packed, which also relates to its function. Here, we found that the PeL microparticle exhibit many crystals with varied orientations of domains, and each of these crystals is composed of domains with a preferential direction. Note that these features are absent in the corresponding brightfield image of the PeL microparticle (Fig. 3(a)).

Next, we performed systematic SHG experiments on glass sample S2. Shown in Fig. 4(a) is a PeL microparticle in sample S2. When the sample was excited by the femtosecond laser, we found that the transversally acquired *xy* nonlinear optical signals from this PeL microparticle (Fig. 4(b)) clearly stand out from the background with about 4 orders of magnitude difference

Optics EXPRESS

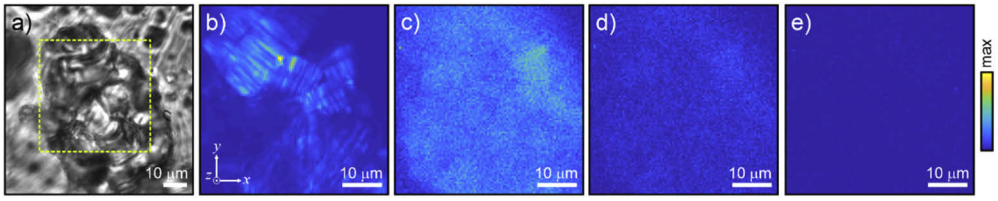

Fig. 3. a) Bright field microscopy image of the PeL microparticle placed on microscopy glass slide (sample S1). b-e) Corresponding transversal *xy* scanning microscopy images of marked region in a) taken with bandpass filter at b) 531 ± 11 nm c) 500 ± 7.5 nm, d) 560 ± 7 nm, and e) 629 ± 28 nm before the photomultiplier tube. In b-e), the image resolution is 100 pixels × 100 pixels, input polarization is linear and input power is 10 mW. The set maxima of intensity scale bars in b) and c-e) are 10000 counts and 100 counts, respectively.

in the respective intensity levels. Here, the background nonlinear optical signals from the bulk glass were found to be close to zero. In this measurement and succeeding measurements, the shortpass filter and the bandpass filter at the SHG wavelength were both kept before the PMT. More importantly, close inspection of the SHG emitting regions in Fig. 4(b) and zoomed region in Fig. 4(c) again revealed several structured domains of varying in-plane orientations in that particular region of the PeL microstructure (as was seen also in sample S1 or Fig. 3(b)). Again, these microscopic features are not visible in the corresponding brightfield microscopy image (Fig. 4(a)).

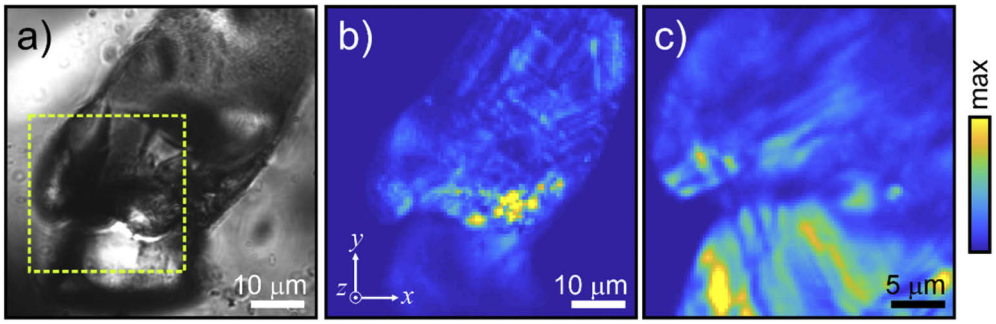

Fig. 4. a) Bright field microscopy image of the PeL microparticle embedded in glass (sample S2). b,c) Transversal *xy* SHG microscopy images of b) overall and c) zoomed regions as shown in Fig. 4(a) and marked region. Image resolution of Figs. 4(b) and 4(c) is 100 pixels × 100 pixels. The SHG images were taken using linear polarization.

The unexpected revelation of structured domains in the PeL microparticle motivated us to further interrogate this unique feature of the PeL microparticle in three dimensions. The three dimensional SHG microscopy images of the marked region in Fig. 4(a) are summarized in Fig. 5. As shown in the transversal *xy* SHG microscopy scans (Figs. 5(a)–5(c)) that were taken at different depths of the sample, the structured domains from different crystal units of the PeL microparticle were found to be spatially distributed in three dimensions. These findings are further evidenced in the corresponding longitudinal *xz* SHG microscopy scans of the sample (Figs. 5(d) and 5(e)). Again, these microscopic features are not visible in the corresponding brightfield microscopy image (Fig. 5(f)). These results strongly establish that SHG microscopy can be used to visualize noninvasively (i.e., no physical cutting of sample) three-dimensionally distributed structured domains in a PeL microparticle.

Optics EXPRESS

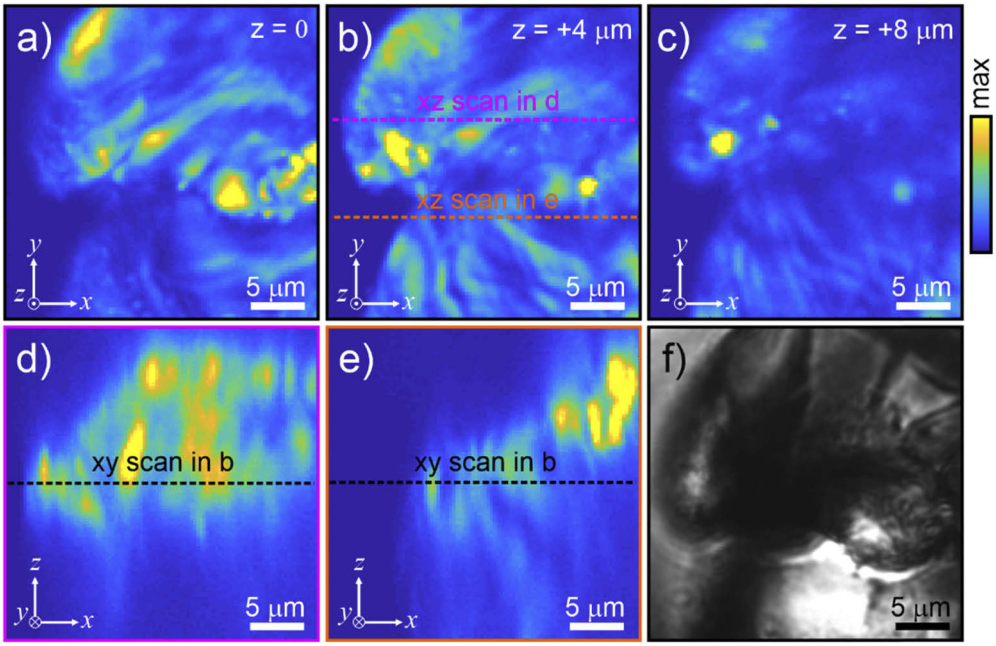

Fig. 5. a-c) Transversal *xy* SHG microscopy images of the marked region in the PeL microparticle as depicted in Fig. 4(a). The SHG images were taken at different focal planes that are separated by 4 μm. d,e) Longitudinal *xz* SHG microscopy images of specific longitudinal planes of the PeL microparticle. The locations of the longitudinal planes are color marked in Fig. 5(b). Image resolution of Figs. 5(a)–5(e) is 100 pixels × 100 pixels. f) Zoomed brightfield microscopy image of Fig. 4(a), which corresponds to the SHG microscopy images in Figs. 5(a)–5(c). The SHG images were taken using circular polarization.

The presence of structured domains inside a crystal unit of PeL material strongly suggests the possibility of small-scale ordered morphologies of the bulk, which cannot be easily accessed by traditional structural characterization techniques that are mostly surface sensitive and also generally destructive. To prove this point, we performed correlated SHG and SEM coupled with EDS experiments on the same PeL microparticle. For this, the PeL microparticles need to be located at the surface of the samples. Shown in Fig. 6(a) is the brightfield microscopy image of the relevant PeL microparticle. The SHG images of the specific regions of interest are shown in Figs. 6(b)–6(h). The SHG images that were taken at different depths (Figs. 6(d)–6(h)) within the sample clearly revealed the presence of structured domains.

However, when the same PeL microparticle (Fig. 6(a)) was examined using SEM with EDS, no corresponding ordered morphologies were seen at the surface of the PeL microparticle (Fig. 7). The elemental maps also revealed that the regions of the PeL microparticle which were probed by SHG are clearly made of Strontium, Aluminum and Dysprosium with no particular spatial distributions that match with the acquired SHG images. This was expected because SEM with EDS has surface sensitive only with very limited depth-discrimination capability. The mapping of Sr and Al confirm the presence of an agglomerate of PeL microparticles.

To date, we are not aware of any other method that has revealed these structured domains inside PeL microparticles. Correlative analyses of the same structures using SHG and other complementary structural imaging techniques are expected to unravel the origin of the SHG sources inside the PeL microparticle. However, there are also limitations in many of the

Optics EXPRESS

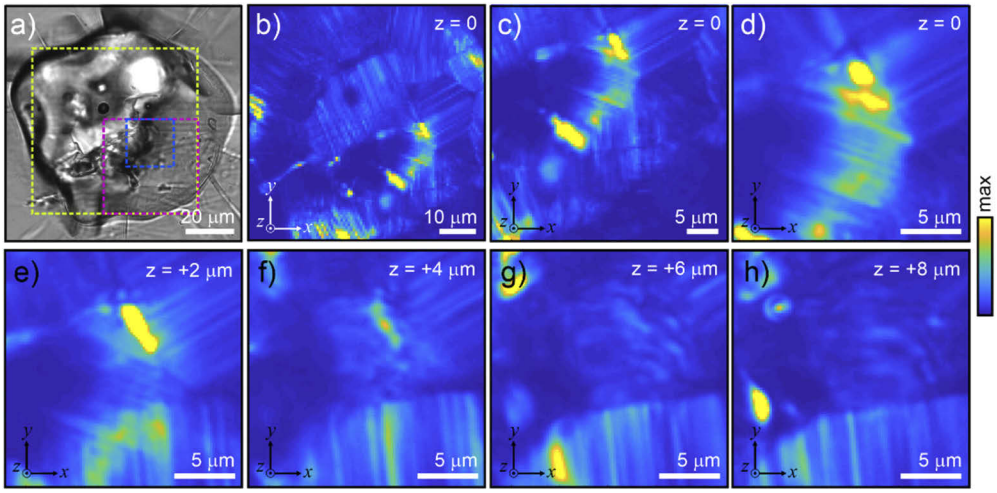

Fig. 6. a) Bright field microscopy image of the PeL microparticle that is located at the polished side of glass sample S2. b,c) Transversal *xy* SHG microscopy images of the marked b) yellow and c) pink colored regions in Fig. 6(a). d-h) Depth-resolved SHG microscopy images of the blue colored region in Fig. 6(a). Here, the SHG images were taken at different focal planes that are separated by 2 µm. Image resolution of Figs. 6(b)–6(h)) is 100 pixels × 100 pixels. The SHG images were taken using circular polarization. The optical slices in Figs. 6(d)–6(h) were used to generate, via ImageJ, a three-dimensional projection of the structured domains (See Visualization 1).

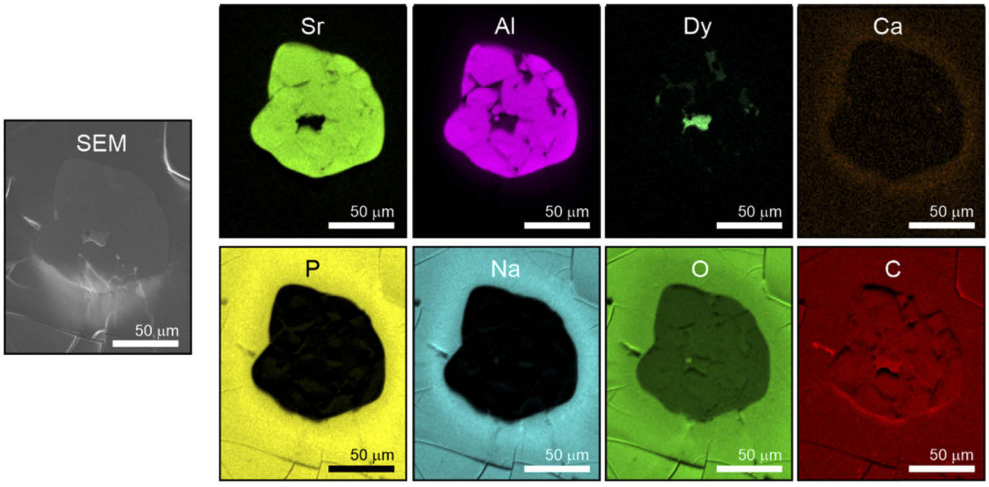

Fig. 7. SEM image and elemental mapping of the PeL microparticle found at the surface of the glass (sample S2). The examined PeL microparticle is the same as in Fig. 6. The maps in Fig. 7 are slightly rotated in-plane with respect to the maps in Fig. 6.

Optics EXPRESS

popular structural imaging techniques (e.g., SEM, TEM, EDS). Imaging such features in their pristine condition and also within the phosphor poses a challenge to such techniques that are only surface-sensitive with very limited depth-discrimination capability and more importantly, destructive. Although it might be possible to probe the structures that are embedded in the phosphor by removing the top layer (e.g., sputtering), the pristine state of the phosphor could be altered as well leading to more complications in the interpretation of origin of microscopic domains. Excluding the optical sectioning effect, the structured domains could be possibly visualized also using birefringence imaging, which relies on structural anisotropy of materials to provide image contrast. However, another limitation is brought about by heterogeneity of the PeL microparticle studied in this work. This will possibly reduce the accuracy of birefringence microscopy especially when quantitative measurements are desired. Finally, the excitation wavelength to be used in birefringence imaging should be carefully selected in order to avoid detection of inherent emission from the PeL microparticles, which are known to be very efficient under typical lighting conditions. Altogether, the results (Figs. 3–7) suggest that SHG microscopy can be used as a new tool to probe the structure of PeL microcrystals in three dimensions and in a noninvasive manner. These previously unseen crystal domains are not accessible in traditional structural characterization techniques like SEM with EDS.

The three-dimensional scans in Figs. 5 and 6 indicate that observed domains from this microparticles might be likely originating from material heterogeneity. This was evidenced by observation of variations in the orientation of domains and of variations in the SHG signals within a particular group of oriented domains as seen in the other optical sections. The microscopic domains of the PeL microparticle could be several microcrystals in contact with each other and with different orientation. More interestingly, each microcrystal exhibits a well-defined orientation appearing visually as a region of alternating SHG signal intensities with some level of periodicity. It is also likely that the dark bands mark boundaries within the crystal sub-units where SHG waves from neighboring emitters interfere destructively. A possible work to be considered in future is to use the microscope to compare the nonlinear optical responses of heterogenous and homogenous phosphors, which are synthesized in different ways. This kind of study is important in investigating the origin of SHG in these structures as well as in opening ways to engineer their respective linear and nonlinear optical responses.

The structured domains in a monoclinic crystal unit of a PeL microparticle have key implications in nonlinear optics, which is not traditionally used to study PeL materials. Our results indicate that PeL microcrystals appear to be SHG-active suggesting that such PeL materials could be used as new nontraditional nonlinear optical materials. The results could also have implications in the characterization and synthesis of old and new phosphors with multifunctional optical properties, e.g., those that exhibit both persistent luminescence and SHG properties. As SHG is very sensitive to symmetry breaking especially at the molecular level, the tailoring of SHG in these new materials could be influenced by the properties of the dopants and host materials. Further tailoring of SHG conversion efficiency is expected from persistent phosphors with highly tunable sizes and shapes including their microscopic assembly and their integration with other photonics materials. Another important implication is that the technique could be developed further in order to detect unambiguously the presence of nanosized PeL emitters in a photonics glass, whose synthesis and characterization remain challenging in practice.

In addition, the revelation of structured domains in the PeL materials using SHG is analogous to the revelation of polar domains that are inherent features of many ferroelectric systems. In fact, such polar domains in ferroelectric materials have been primarily investigated by SHG [27]. Polarization analysis of SHG is indeed useful in identifying the crystallization and orientation of these PeL microcrystals in detail. However, the polarization analysis is beyond the scope of the present work and will be considered in a follow-up study. In the future, we plan to further investigate the SHG response of a PeL crystal in detail (e.g., quantitatively) using

Optics EXPRESS

polarization-resolved SHG microscopy, where the SHG signals are analyzed in detail. Due to the extreme sensitivity of SHG to the crystallographic structure of materials and the spatial symmetry of the environment, we also expect that SHG microscopy could provide a noninvasive way to study polymorphs, symmetry sites, strain, size, and defects of PeL materials that are embedded in different glass matrices. Together with the development of novel combinations of PeL materials and glass matrices, SHG microscopy could also offer new information about the links of persistent luminescence and SHG in related materials supporting lattice strains that occur when rare-earth ions are substituted into host crystals [39]. Previously, such approach has been found to significantly influence the SHG properties of different host materials [40–42]. As shown in our SHG verification measurements in Fig. 3, we barely detected the nonlinear optical signals at the wavelengths that are longer than the expected SHG wavelength. This suggests that two-photon resonance could be very weak to be collected by our microscopy system. However, the possibility of two-photon resonance excitation in this material and its link to SHG efficiency could be an important subject to investigate in the future. In this kind of work, SHG microscopy at different excitation wavelengths should be performed.

As in other kinds of optical microscopy techniques, the image quality and three-dimensional optical sectioning capability of the SHG microscopy technique could be further improved by increasing the spatial resolution of the microscope. Conventionally, this can be achieved by using short excitation wavelengths. In addition, a high numerical aperture immersion objective could be used to reduce the focal spot size. However, the latter should be carefully considered since the immersion oil could disturb a hygroscopic glass sample. This is especially critical for the characterization of those PeL microparticles that are found on top of the glass substrate and require further characterization with other instruments (e.g., SEM and EDS). Using our present numerical aperture of 0.8, we have been able to achieve a spot size of about 1 micron. The resulting image quality is sufficient to address these microstructures in a nondestructive manner and in three dimensions.

4. Summary and outlook

We demonstrated the use of SHG microscopy to investigate individual persistent luminescent microparticles that are either as prepared on top of glass or embedded in glass. Three-dimensional mapping of the second-harmonic generation from monoclinic dysprosium- and europium-doped strontium aluminates, a popular persistent luminescent material, allowed us to unambiguously visualize and reveal for the first time the presence of micrometer-sized domains from such microparticles. This information could be important for the society of persistent phosphors because the technique can be used to probe nondestructively the microscopic domains within the PeL particle, which is difficult to do in practice. Equivalently, the observation of SHG in this material could be important for the community of nonlinear nanophotonics, where the search of new SHG-active materials is always desired. The technique is expected to mature as a complementary optical microscopy technique to study noninvasively a wide array of persistent luminescent entities at the individual particle level. We hope that the technique could be used in order to complement our understanding of persistent phosphors through the viewpoint of nonlinear optical microscopy.

Funding

Academy of Finland (Academy Project (No. 316483), Academy Project (No. 326418), PREIN Flagship Programme (No. 320165)).

Optics EXPRESS

Acknowledgments

This work made use of Tampere Microscopy Center facilities at Tampere University, especially the authors would like to thank Dr. T. Salminen for collecting the elemental mappings.

Disclosures

The authors declare no conflicts of interest.

References

1. T. Aitasalo, P. Dereń, J. Hölsä, H. Jungner, J.-C. Krupa, M. Lastusaari, J. Legendziewicz, J. Niittykoski, and W. Stręk, "Persistent luminescence phenomena in materials doped with rare earth ions," J. Solid State Chem. **171**(1-2), 114–122 (2003).
2. T. Matsuzawa, Y. Aoki, N. Takeuchi, and Y. Murayama, "A new long phosphorescent phosphor with high brightness, SrAl2O4: Eu2+, Dy3+," J. Electrochem. Soc. **143**(8), 2670–2673 (2019).
3. T. Aitasalo, J. Hölsä, H. Jungner, M. Lastusaari, and J. Niittykoski, "Thermoluminescence study of persistent luminescence materials: Eu 2+- and R3+-doped calcium aluminates, CaAl 2O4:Eu2+,R3+," J. Phys. Chem. B **110**(10), 4589–4598 (2006).
4. Q. L. M. De Chermont, C. Chanéac, J. Seguin, F. Pellé, S. Maîtrejean, J. P. Jolivet, D. Gourier, M. Bessodes, and D. Scherman, "Nanoprobes with near-infrared persistent luminescence for in vivo imaging," Proc. Natl. Acad. Sci. U. S. A. **104**(22), 9266–9271 (2007).
5. T. Maldiney, A. Bessière, J. Seguin, E. Teston, S. K. Sharma, B. Viana, A. J. J. Bos, P. Dorenbos, M. Bessodes, D. Gourier, D. Scherman, and C. Richard, "The in vivo activation of persistent nanophosphors for optical imaging of vascularization, tumours and grafted cells," Nat. Mater. **13**(4), 418–426 (2014).
6. J. Liu, T. Lécuyer, J. Seguin, N. Mignet, D. Scherman, B. Viana, and C. Richard, "Imaging and therapeutic applications of persistent luminescence nanomaterials," Adv. Drug Delivery Rev. **138**, 193–210 (2019).
7. T. Maldiney, B. Ballet, M. Bessodes, D. Scherman, and C. Richard, "Mesoporous persistent nanophosphors for in vivo optical bioimaging and drug-delivery," Nanoscale **6**(22), 13970–13976 (2014).
8. C. N. Xu, T. Watanabe, M. Akiyama, and X.-G. Zheng, "Direct view of stress distribution in solid by mechanoluminescence," Appl. Phys. Lett. **74**(17), 2414–2416 (1999).
9. Y. Li, M. Gecevicius, and J. Qiu, "Long persistent phosphors - From fundamentals to applications," Chem. Soc. Rev. **45**(8), 2090–2136 (2016).
10. K. D. Vernon-Parry, "Scanning electron microscopy: an introduction," III-Vs Rev. **13**(4), 40–44 (2000).
11. M. Eckert, "Max von Laue and the discovery of X-ray diffraction in 1912," Ann. Phys. **524**(5), A83–A85 (2012).
12. R. Fitzgerald, K. Keil, and K. F. J. Heinrich, "Solid-State Energy-Dispersion Spectrometer for Electron-Microprobe X-ray Analysis," Science **159**(3814), 528–530 (1968).
13. R. E. Rojas-Hernandez, F. Rubio-Marcos, R. H. Gonçalves, MÁ Rodriguez, E. Véron, M. Allix, C. Bessada, and J. F. Fernandez, "Original Synthetic Route to Obtain a SrAl2O4 Phosphor by the Molten Salt Method: Insights into the Reaction Mechanism and Enhancement of the Persistent Luminescence," Inorg. Chem. **54**(20), 9896–9907 (2015).
14. K. Pavani, J. S. Kumar, T. Sasikala, B. C. Jamalaiah, H. J. Seo, and L. R. Moorthy, "Luminescent characteristics of Dy3+ doped strontium magnesium aluminate phosphor for white LEDs," Mater. Chem. Phys. **129**(1-2), 292–295 (2011).
15. S. Carlson, J. Hölsä, T. Laamanen, M. Lastusaari, M. Malkamäki, J. Niittykoski, and R. Valtonen, "X-ray absorption study of rare earth ions in Sr2MgSi2O7:Eu2+,R3+ persistent luminescence materials," Opt. Mater. (Amsterdam, Neth.) **31**(12), 1877–1879 (2009).
16. R. W. Boyd, *Nonlinear Optics* (Academic Press, 2008).
17. S. Brasselet, "Polarization-resolved nonlinear microscopy: application to structural molecular and biological imaging," Adv. Opt. Photonics **3**(3), 205–271 (2011).
18. G. Bautista and M. Kauranen, "Vector-field nonlinear microscopy of nanostructures," ACS Photonics **3**(8), 1351–1370 (2016).
19. A. Podlipensky, J. Lange, G. Seifert, H. Graener, and I. Cravetchi, "Second-harmonic generation from ellipsoidal silver nanoparticles embedded in silica glass," Opt. Lett. **28**(9), 716–718 (2003).
20. E. Delahaye, N. Tancrez, T. Yi, I. Ledoux, J. Zyss, S. Brasselet, and R. Clement, "Second harmonic generation from individual hybrid MnPS3-based nanoparticles investigated by nonlinear microscopy," Chem. Phys. Lett. **429**(4-6), 533–537 (2006).
21. J. Butet, J. Duboisset, G. Bachelier, I. Russier-Antoine, E. Benichou, C. Jonin, and P.-F. Brevet, "Optical Second Harmonic Generation of Single Metallic Nanoparticles Embedded in a Homogeneous Medium," Nano Lett. **10**(5), 1717–1721 (2010).
22. K. Mishchik, Y. Petit, E. Brasselet, A. Royon, T. Cardinal, and L. Canioni, "Patterning linear and nonlinear optical properties of photosensitive glasses by femtosecond structured light," Opt. Lett. **40**(2), 201–204 (2015).

Optics EXPRESS

23. M. A. van der Veen, F. Vermoortele, D. E. De Vos, and T. Verbiest, "Point Group Symmetry Determination via Observables Revealed by Polarized Second-Harmonic Generation Microscopy: (1) Theory," Anal. Chem. **84**(15), 6378–6385 (2012).
24. P. D. Schmitt, E. L. Dewalt, X. Y. Dow, and G. J. Simpson, "Rapid Discrimination of Polymorphic Crystal Forms by Nonlinear Optical Stokes Ellipsometric Microscopy," Anal. Chem. **88**(11), 5760–5768 (2016).
25. J. Kaneshiro, S. Kawado, H. Yokota, Y. Uesu, and T. Fukui, "Three-dimensional observations of polar domain structures using a confocal second-harmonic generation interference microscope," J. Appl. Phys. **104**(5), 054112 (2008).
26. K. Markey, T. Putzeys, P. Horcajada, T. Devic, N. Guillou, M. Wübbenhorst, S. Van Cleuvenbergen, T. Verbiest, D. E. De Vos, and M. A. Van Der Veen, "Second harmonic generation microscopy reveals hidden polar organization in fluoride doped MIL-53(Fe)," Dalton Trans. **45**(10), 4401–4406 (2016).
27. S. A. Denev, T. T. A. Lummen, E. Barnes, A. Kumar, and V. Gopalan, "Probing ferroelectrics using optical second harmonic generation," J. Am. Ceram. Soc. **94**(9), 2699–2727 (2011).
28. G. Bautista, C. Dreser, X. Zang, D. P. Kern, M. Kauranen, and M. Fleischer, "Collective Effects in Second-Harmonic Generation from Plasmonic Oligomers," Nano Lett. **18**(4), 2571–2580 (2018).
29. L. Turquet, J.-P. Kakko, X. Zang, L. Naskali, L. Karvonen, H. Jiang, T. Huhtio, E. Kauppinen, H. Lipsanen, M. Kauranen, and G. Bautista, "Tailorable second-harmonic generation from an individual nanowire using spatially phase-shaped beams," Laser Photonics Rev. **11**(1), 1600175 (2017).
30. G. Bautista, J.-P. Kakko, V. Dhaka, X. Zang, L. Karvonen, H. Jiang, E. Kauppinen, H. Lipsanen, and M. Kauranen, "Nonlinear microscopy using cylindrical vector beams: Applications to three-dimensional imaging of nanostructures," Opt. Express **25**(11), 12463–12468 (2017).
31. L. Turquet, X. Zang, J.-P. Kakko, H. Lipsanen, G. Bautista, and M. Kauranen, "Demonstration of longitudinally polarized optical needles," Opt. Express **26**(21), 27572–27584 (2018).
32. P. Kunwar, J. Toivonen, M. Kauranen, and G. Bautista, "Third-harmonic generation imaging of three-dimensional microstructures fabricated by photopolymerization," Opt. Express **24**(9), 9353–9358 (2016).
33. H. Nguyen, M. Tuomisto, J. Oksa, T. Salminen, M. Lastusaari, and L. Petit, "Upconversion in low rare-earth concentrated phosphate glasses using direct NaYF4:Er3 +, Yb3 + nanoparticles doping," Scr. Mater. **139**, 130–133 (2017).
34. N. Ojha, M. Tuomisto, M. Lastusaari, and L. Petit, "Phosphate glasses with blue persistent luminescence prepared using the direct doping method," Opt. Mater. (Amsterdam, Neth.) **87**, 151–156 (2019).
35. R. E. Rojas-Hernandez, F. Rubio-Marcos, A. Serrano, A. Rakhmatullin, C. Bessada, and J. F. Fernandez, "Unveiling the role of the hexagonal polymorph on SrAl2O4-based phosphors," RSC Adv. **8**(51), 28918–28927 (2018).
36. G. Wang, J. Lu, D. Cui, Z. Xu, Y. Wu, P. Fu, X. Guan, and C. Chen, "Efficient second harmonic generation in a new nonlinear La2CaB10O19 crystal," Opt. Commun. **209**(4-6), 481–484 (2002).
37. Y. Liu, L. Wei, F. Yu, Z. Wang, Y. Zhao, S. Han, X. Zhao, and X. Xu, "Crystal growth and efficient second-harmonic-generation of the monoclinic LaCa4O(BO3)3 crystal," CrystEngComm **15**(30), 6035–6039 (2013).
38. E. Boursier, P. Segonds, J. Debray, P. L. Inácio, V. Panyutin, V. Badikov, D. Badikov, V. Petrov, and B. Boulanger, "Angle noncritical phase-matched second-harmonic generation in the monoclinic crystal BaGa4Se7," Opt. Lett. **40**(20), 4591 (2015).
39. P. D. Townsend, A. K. Jazmati, T. Karali, M. Maghrabi, S. G. Raymond, and B. Yang, "Rare-earth-size effects on the thermoluminescence and second-harmonic generation," J. Phys.: Condens. Matter **13**(10), 2211–2224 (2001).
40. D. Hreniak, W. Strek, A. Speghini, M. Bettinelli, G. Boulon, and Y. Guyot, "Infrared induced red luminescence of Eu3+ -doped polycrystalline LiNbO3," Appl. Phys. Lett. **88**(16), 161118 (2006).
41. D. M. Krol and J. R. Simpson, "Photoinduced second-harmonic generation in rare-earth-doped aluminosilicate optical fibers," Opt. Lett. **16**(21), 1650–1652 (1991).
42. T. K. Yadav, A. K. Singh, K. Kumar, and R. A. Yadav, "Luminescence and second harmonic generation in Eu3+/Eu 2+ embedded B2O3: LiNbO3 non-linear glass-ceramics," Opt. Mater. (Amsterdam, Neth.) **33**(11), 1732–1736 (2011).